Pressure-Driven Insulin Release Overcomes Limitations of Diffusion for Encapsulated Islet Cell Therapy

Ella A. Thomson[1], Rayhan A. Lal[2,3,4], Haixia Xu[2], Sooyeon Lee[2], Hannah Moeller[4,5], Justin P. Annes[2,4]*, Ada S. Y. Poon[1]*

[1]Department of Electrical Engineering, Stanford University, Stanford, CA 94305, USA.

[2]Division of Endocrinology, Department of Medicine, Stanford University, Stanford, CA 94305, USA.

[3]Division of Endocrinology, Department of Pediatrics, Stanford University, Stanford, CA 94305, USA.

[4]Stanford Diabetes Research Center, Stanford, CA 94305, USA.

[5]Department of Chemical and Systems Biology, Stanford University, Stanford, CA 94305, USA.

*Corresponding author. Email: adapoon@stanford.edu and jannes@stanford.edu

One Sentence Summary:

Diffusion-based insulin delivery from macroencapsulated islet cells is incompatible with physiologic glucose control, a constraint addressed through pressure-based insulin delivery.

Abstract:

Cadaveric islet and stem cell-derived transplantation show great promise as therapeutic approaches for type 1 diabetes. To address the immunocompatibility challenge, numerous cellular macroencapsulation techniques, which rely upon diffusion to transport insulin across the immunoprotective barrier, have been proposed. Although several of these devices were advanced to human clinical trials, they uniformly failed to achieve physiologic glucose control or insulin independence. Indeed, based upon mathematical modeling and empiric evidence, diffusion-based encapsulation devices are fundamentally incompatible with homeostatic on-demand insulin delivery and physiologic glucose regulation. To realize the potential of achieving insulin independence through macroencapsulated cell-based therapy, we propose the necessity of a second driving force. Herein, we provide both theoretical proof and experimental demonstration that modest (11-kPa) micropump-applied pressure considerably enhances insulin flux across immunoisolation membranes by nearly three orders of magnitude, enabling precise delivery of both bolus and basal insulin. Furthermore, pressure-driven insulin efflux from encapsulated mouse and human islets is fast and repeatable. As such, we urge caution against further advancement of diffusion-based immune-isolating macroencapsulation devices that do not incorporate a secondary driving force for precise temporal regulation of peptide delivery.

INTRODUCTION

Type 1 diabetes (T1D) is characterized by autoimmune islet beta-cell destruction and insulin deficiency. Current treatment utilizes exogenous insulin administered *via* subcutaneous injection or infusion. Automated insulin dosing (AID) is increasingly common but still limited in efficacy and uptake[1], particularly among racial and ethnic minorities[2]. Additionally, T1D treatment remains burdensome, costly, and associated with acute, life-threatening hypoglycemia. Individuals living with diabetes require frequent or continuous glucose monitoring, wearing a pump or administering injections, and accounting for carbohydrate ingestion and activity that alters insulin sensitivity[3]. Alternatively, islet transplantation could alleviate patient management burden and cost. In perhaps the simplest incarnation, allogeneic islets are infused into the liver *via* the portal vein[4–6]. While this approach fosters islet function and viability, providing insulin independence in the short term, transplants generally fail due to immunosuppressive toxicity and insufficiency[4,5]. Recently, the VX-880 (hepatic portal vein infusion of fully differentiated allogeneic stem cell-derived insulin-producing islet cells) found success in clinical trials, with two people achieving insulin independence[7,8]. However, the need for immunosuppression remains a barrier to widespread deployment. Islet encapsulation has been introduced to circumvent the challenge of immunocompatibility. Nano- and micro-encapsulation can improve immunocompatibility; however, microcapsules have difficulty achieving full immunoisolation[9–11], and because these transplants are not retrievable, safety concerns remain. Vascularized islet transplants such as the ViaCyte VC-02 and the Sernova cell pouch allow for retrieval while still permitting direct nutrient, glucose, and insulin transfer from/to the circulation[12–15], and have reached the stage of human clinical trials. While increased C-peptide levels were observed with these devices, insulin independence was not achieved[12,13]. Additionally, the need for immunosuppression limits the broad applicability of this approach.

Macroencapsulation strategies, which provide both immune isolation and retrievability, are among the most actively pursued transplantation approaches. Numerous porous membranes and macrobeads have been investigated, with select systems advancing to clinical evaluation[16–24]. While encapsulation provides a beneficial physical barrier against host immune cell entry, this immunoprotective barrier also impedes the movement of insulin[25–27]. Relying solely on diffusion for insulin transport is insufficient to achieve physiologic glucose control or insulin independence. For instance, with islets enclosed by a standard porous Polyethylene terephthalate (PET) membrane of area 25 cm^2, diffusion alone would require approximately 6 hours to transport a human-sized insulin bolus. Notably, the potential for increasing insulin transport through novel membrane design, a significant area of investigation, is limited. Furthermore, the use of cell stimulation[28] alone is inadequate to overcome this limitation.

Diffusion-based encapsulation is fundamentally incompatible with achieving homeostatic on-demand insulin delivery and physiologic glucose regulation. This critical limitation has been obfuscated by an extensive body of literature that has "validated" islet encapsulation approaches in mice *via* improved or normalized glucose tolerance, without corresponding rescue of insulin

and/or C-peptide release. These publications neglect the well-described phenomenon of glucose effectiveness—the ability of glucose to influence its own disposal and hepatic glucose output[29,30]. Glucose effectiveness exhibits greater prominence in rodents compared to humans[31–33], with the magnitude of this difference being at least twice as significant[34]. In streptozotocin (STZ)-induced diabetic rodents, implantation of an insulin pellet, which provides only basal insulin, combined with glucose effectiveness is sufficient to normalize glucose tolerance testing[31]. Similarly, when the Beta-Air device, which is immunoisolating, was implanted in diabetic rodents, normal glucose tolerance test results were achieved, with no data presented on either insulin or C-peptide release[35]. However, recent clinical trials of the Beta-Air device in humans fail to demonstrate therapeutic glucose control and insulin independence[20,22]. Therefore, achieving a normal glucose tolerance test, particularly in rodents, does not affirm an appropriate insulin secretion response necessary for human efficacy.

Reliance on diffusion and rodent glucose tolerance testing has stifled progress in the field of encapsulated islet transplantation. To realize the potential of achieving insulin independence through macroencapsulated cell-based therapy, we propose the necessity of a second driving force to increase and control insulin transport kinetics (Fig. 1a). Our theoretical analysis and experimental findings confirm that the application of a modest (~11-kPa) applied pressure—roughly equivalent to normal diastolic blood pressure in humans—rapidly and efficiently facilitates insulin flux across encapsulating membranes. This pressure-based dosing method enables sub-minute insulin release, resembling the behavior of native islets or exogenous infusions, and allows for repeated bolus insulin delivery. By harnessing this second driving force, we acutely restored euglycemia in mice with complete or near-complete lack of endogenous insulin production within a timeframe unattainable through diffusion alone.

RESULTS

Proof of the effect of applied pressure on insulin transport across porous membranes

To describe how applied pressure is a feasible second driving force, we consider the simultaneous effect of pressure (p) and concentration (c_s) gradients on the transport of insulin across a porous membrane. The insulin (solute) flux, J_s, is the combined effect of the solute diffusional flow and the driving force from the volumetric solvent flux, J_v. The solute diffusional flow $-D_s \nabla c_s$ is driven by the insulin concentration gradient where D_s is the insulin diffusion coefficient. The volumetric solvent flux is a pressure-driven flow; this flow in turn carries the insulin to flow through the membrane resulting in an insulin flux of $J_v c_s = -L_p h \nabla p \cdot c_s$ where L_p is the filtration coefficient and h is the membrane thickness. Here, we are interested in finding a simple expression for the ratio of the insulin flux with and without the applied pressure in steady state to comprehend the multiplicative effect of applied pressure relative to diffusion alone for insulin transport. This expression is given by

$$\frac{P_e}{1 - e^{-P_e}} \cdot \frac{c_{s,in} - c_{s,out} e^{-P_e}}{c_{s,in} - c_{s,out}} \approx P_e \tag{1}$$

where $c_{s,in}$ and $c_{s,out}$ are the insulin concentration inside and outside the encapsulation respectively. In the ratio, P_e is the axial Peclet number defined by $P_e = \frac{L_p h \Delta p}{D_s}$. When P_e is large, the ratio in Eq. 1 approximates to P_e; that is, the Peclet number alone reveals the multiplicative effect of applied pressure relative to diffusion for insulin transport.

For insulin transport where membrane pore radius (r_p) is much greater than molecular radius of insulin (r_s), we apply the Hagen-Poiseuille Law and Strokes-Einstein Equation to obtain

$$P_e = \frac{3\pi r_s}{4 k_B T} \cdot r_p^2 \cdot \Delta p \ = \ 7.36 \times 10^{11} \cdot r_p^2 \cdot \Delta p \tag{2}$$

where k_B is the Boltzmann constant and T is the absolute temperature. Here, we showed that the multiplicative effect of applied pressure compared to diffusion alone on insulin transport is primarily determined by two key factors: the membrane's pore radius and the magnitude of the applied pressure. For typical insulin transport membranes (pore radius ~ sub-μm), this ratio approximates to $0.1\Delta p$. That is, a 11-kPa applied pressure (roughly equivalent to normal diastolic blood pressure in humans) will increase steady-state insulin flux by ~3 orders of magnitude. During transient transport, this multiplicative effect in insulin flux translates into a scaling of release time. An 11-kPa applied pressure takes 3 orders of magnitude less time to transport the same amount of insulin for a given membrane area. Furthermore, a 11-kPa pressure may be provided by a range of micropumps[36–38] with dimensions less than a few centimeters in size, suitable for implantation in humans.

Numerical simulation and measurement of insulin flux through an encapsulation membrane with and without a small pressure gradient

We performed numerical simulations of insulin transport assuming a membrane area in the range of square centimeters. Our results revealed that when relying solely on diffusion, it took over 2 hours to transport > 90% of the encapsulated insulin (Fig. 1a, b). However, when an 11-kPa pressure was applied, the transport time was significantly reduced to approximately 10 seconds (Fig. 1c), confirming the accuracy of our theoretical findings.

To further validate our theoretical findings, we conducted experimental studies using a porous PET membrane (0.4-µm pore diameter, 12% porosity) commonly used for encapsulation[16,17,28]. These experiments were performed in a 12-well format, both with and without the application of an applied pressure using a piezoelectric micropump (Fig. 1d and Supplementary Fig. 1). The empirical results were concordant with our model-based predictions (Fig. 1e, f), and were consistent across a range of pore sizes, porosities, and membrane compositions (Fig. 1g and Supplementary Fig. 2). For pore sizes ranging from 0.2 to 0.8 µm, applied pressure increased flux by an average of ~400-fold over diffusion (Fig. 1g). Additionally, an average pressure of ~11 kPa at the membrane was empirically confirmed (Supplementary Fig. 3) without any observed backflow. Notably, a modest applied pressure greatly reduced the time required to transport encapsulated insulin, from several hours for diffusion alone, to less than a minute.

In vitro validation of insulin bolus delivery from encapsulated R7T1 pseudoislets and human islets

Based on the above findings, we hypothesized that the encapsulation membrane hinders diffusion-dependent insulin delivery from secretagogue-stimulated β-cells; and a modest pressure can generate insulin boluses independent of cell stimulation such as glucose-stimulated insulin secretion (GSIS) and KCl-triggered insulin secretion. To test this hypothesis, we measured insulin delivery from encapsulated R7T1 β-cell pseudoislets (Fig. 2a). R7T1 cells were characterized by measuring proliferating and growth arrested insulin secretion (Supplementary Fig. 4). Approximately 800 pseudoislets were encapsulated in porous PET (Fig. 2b) and exposed to basal [5 mM glucose] or stimulatory [40 mM KCl] culture conditions. As expected, 15 minutes of KCl treatment significantly increased total insulin release ($p < 0.0001$; Fig. 2c, d). We chose the 15-minute time point to approximate the suggested pre-meal insulin bolus injection time in individuals with T1D. However, when relying upon diffusion alone, KCl treatment did not significantly increase insulin levels outside of encapsulation compared to basal levels ($p > 0.9$; Fig. 2d). In contrast, when a second driving force, a modest applied pressure, was introduced for 30 seconds, there was a substantial increase in insulin levels outside the encapsulation ($p < 0.0001$; Fig. 2c, d). These data clearly demonstrated that KCl exposure effectively triggered insulin release from pseudoislets; however, a corresponding rise of insulin outside the encapsulation, on a physiologically relevant time scale, was not achieved unless a second driving force was applied.

These results corroborated previously reported findings of limited insulin release on a physiological time scale from encapsulated, electrically stimulated cells[28].

To extend these findings, we compared diffusion and pressure-driven insulin efflux from encapsulated pseudoislets over 8 hours. As predicted, an ~11-kPa applied pressure yielded nearly 3 orders of magnitude higher insulin flux than diffusion alone (Fig. 2e). This clearly demonstrated that the application of a second driving force (pressure) enabled rapid bolus delivery of insulin within a sub-minute timeframe, independent of cell stimulation. To evaluate potential adverse effects of applied pressure on β-cell health and function, we performed three successive pressure-driven doses at 8-hour intervals. No decrement in insulin release occurred across consecutive doses (Fig. 2f), indicating that pseudoislets remained functional even after pressure-driven dosing. Notably, diffusion-dependent insulin delivery was similarly stable, though reduced by three orders of magnitude compared to pressure-driven delivery (Fig. 2f). We also performed measurements to determine the effect of R7T1 pseudoislet number on insulin secretion. As expected, insulin secretion increased linearly with pseudoislet number (Supplementary Fig. 5).

Additionally, we investigated the viability of encapsulated primary human islets *in vitro* over a 5-day period and found similarly preserved viability with both diffusion and pressure-based insulin delivery methods (Supplementary Fig. 6). Collectively, these data indicated that applied pressure did not negatively impact the health of R7T1 pseudoislets or primary human islets. Moreover, pressure-driven dosing yielded repeated and consistent stimulation-independent bolus insulin delivery. This property is advantageous for the development of cell-based therapies by avoiding previously (qualitatively) described delay[26].

In vivo validation on insulin bolus delivery using wild type mice

Having established *in vitro* validation, we proceeded to evaluate the feasibility of pressure-driven insulin dosing *in vivo*. Wild type mice (C57BL/6J) were subcutaneously implanted with encapsulated mouse islets (Fig. 3a). The implants used in all *in vivo* experiments were well tolerated, as indicated by H&E staining (Supplementary Fig. 7), and consistent with previously described implantable devices[39]. Pressure-based dosing was performed immediately after device implantation. The average starting blood glucose, following anesthesia, was 286 mg/dL. To ensure accurate interpretation of glucose effectiveness, we tracked both blood insulin and blood glucose after implantation and dosing (Fig. 3b). Thirty seconds of ~11-kPa applied pressure was utilized for insulin bolus delivery from a 200-μL implant. The blood insulin level in mice dosed by applied pressure was 35-fold higher than in animals treated by diffusion at 30 minutes (Fig. 3c). Consequently, blood glucose levels decreased by an average of 229 mg/dL with pressure-driven dosing as compared to 47 mg/dL with diffusion at 60 minutes (Fig 3d). Analysis of the encapsulation device revealed that approximately 90% of the insulin secreted by the mouse islets remained within the device after diffusion-based delivery, while less than 10% remained after pressure-driven delivery method (Fig. 3e). Moreover, the blood insulin AUC was ~32-fold higher in animals treated with pressure-driven *versus* diffusion-based delivery (Fig. 3f). These findings

demonstrated that pressure was required to generate a physiologically relevant insulin bolus *in vivo*.

Restoring euglycemia in diabetic mice through pressure-driven insulin dosing

To evaluate the translational potential of pressure-driven insulin dosing, we performed *in vivo* transplantation experiments with encapsulated mouse and human islets in STZ-induced diabetic mice. Dosing was performed immediately after device implantation. The blood insulin level in mice dosed by applied pressure showed a substantial increase, with an average of 5.4 ng/mL for mouse islets and 7.6 ng/mL for human islets (xenogenic transplantation) within 30 minutes (Fig. 4a, b left). In contrast, animals treated with diffusion alone exhibited a much lower increase in blood insulin levels during the same time period, with an average of 0.04 ng/mL for mouse islets and 0.38 ng/mL for human islets. By 60 minutes, blood glucose levels decreased by an average of 368 mg/dL from mouse islets and 426 mg/dL from human islets with pressure-driven dosing as compared to an average of 30 mg/dL and 57 mg/dL, respectively, with diffusion (Fig. 4a, b right). Notably, mice treated with pressure-driven dosing reached euglycemia within 60 minutes, an outcome that was not attained through diffusion-dependent insulin delivery from encapsulated islets. While bolus delivery was not achieved by diffusion alone, some impact on blood insulin was observed by 60 minutes (p = 0.03 for human islets; Fig. 4b). Together these results demonstrated that applied pressure overcame the profound limitation imposed by diffusion, enabling efficient bolus insulin delivery.

Next, we evaluated whether a renewable and expandable insulin source, reversibly transformed mouse R7T1 pseudoislets (which can be proliferated as needed), could achieve blood glucose control in STZ-induced hyperglycemic mice. Using pressure-driven dosing, blood glucose decreased by an average of 108 mg/dL at 60 minutes. However, when mice were treated by diffusion, blood glucose rose by an average of 32 mg/dL, potentially due to the diffusion of glucose from the encapsulated cell media (Fig. 4c). These data are consistent with the slight glucose increase observed in Fig. 3d. Our results indicated that by employing pressure-based dosing, glucose control was improved with a readily accessible, renewable, and titratable β-cell line; an alternative to harvested mouse islets, human islets, or stem-cell derived pancreatic cells.

Improving glycemic control in diabetic mice with repeated pressure-driven insulin boluses and basal insulin delivery

To provide translational relevance of pressure-driven insulin delivery, we tested its ability to acutely improve blood glucose homeostasis in mice with diabetes *via* repeated bolus insulin dosing (Fig. 5a). Within 30 minutes of the first pressure-driven bolus, blood glucose dropped by an average of 310 mg/dL; in contrast, mice treated with diffusion alone rose by an average of 41 mg/dL (Fig. 5b and Supplementary Fig. 8). Sham controls showed an average decrease of 21 mg/dL in blood glucose, confirming that the substantial glucose drop in transplanted mice was due

to released insulin. Importantly, the observed kinetics are consistent with the pharmokinetic profile of subcutaneously dosed regular insulin[40]. After 6 hours, a second dose was administered, and consistent with our *in vitro* findings, a similar reduction in glucose levels was observed with pressure delivery, with an average decrease of 270 mg/dL, while diffusion led to an average increase of 32 mg/dL (Fig. 5c). Total AUC of delta blood glucose in mice treated with applied pressure was dramatically reduced to −180,560 ± 35,003 compared to mice treated by diffusion alone, which had an AUC of −18,549 ± 11,338 (Fig. 5d). Notably, animals were freely eating and drinking between dosing, emphasizing the effectiveness and stability of pressure-driven insulin delivery. Additionally, by the end of the experiment (6 hours after the last dose had been delivered), all animals had returned to a state of hyperglycemia (521 +/- 35 mg/dl). This indicates that the restoration of euglycemia observed in pressure treated mice was due to the pressure delivered doses and not endogenous insulin production.

Finally, we demonstrated the versatility of pressure-based dosing by using it for both basal insulin delivery and bolus delivery. Here, we developed a wireless wearable micropump system to repeatedly deliver basal insulin *via* pressured-based dosing in freely behaving mice, with no need for tethering or repeated anesthesia (Fig. 5e and Supplementary Movie 1). The system consisted of a piezoelectric micropump, a dual channel pump driver, a BLE controller, and a 1-mL reservoir, and was powered from a single coin-cell battery (Fig. 5f and Supplementary Fig. 9). An initial subcutaneous insulin injection of 0.05 units was administered to lower blood glucose levels, followed by either diffusion- or pressure-driven insulin delivery to maintain blood glucose levels (Fig. 5g). The total blood glucose AUC was –2556 for pressure-based dosing and –804 for controls (Fig. 5h and Supplementary Fig. 10; $p < 0.001$). This significant decrease in blood glucose AUC demonstrated that pressure-based basal insulin delivery effectively maintained euglycemia in mice with severe diabetes. Moreover, this experiment highlighted the feasibility of performing pressure-based delivery in freely behaving mice, without the need for anesthesia or tethering.

DISCUSSION

For several decades, immunoisolated macroencapsulated islet transplantation has held promise for revolutionizing T1D treatment; unfortunately, this approach has been disappointingly unsuccessful. While some systems have demonstrated somewhat elevated circulating C-peptide or insulin levels in transplanted models, insulin independence has not been realized[12,13]. Critically, insulin transport kinetics were generally overlooked in these studies; the problematic and consistent observation that these devices, which rely upon diffusion for insulin delivery, fail to provide substantial nutrient-responsive insulin dosing has been assiduously downplayed[25,26]. In this work, we directly confront this profound impediment to progress and acknowledge the need to introduce a second driving force to enable on-demand insulin dosing. We conclusively demonstrate that diffusion is incompatible with releasing insulin from encapsulated islets/β-cells on a sub-minute time scale and propose a potential solution that utilizes a small pressure gradient as a second driving force for insulin transport. Importantly, we avoid reliance on glucose tolerance testing to prevent misinterpretation of results due to glucose effectiveness. We demonstrate that this applied pressure does not decrease viability of transplanted cells relative to diffusion alone. This approach allows for rapid insulin dosing from encapsulated islets on a time scale that reflects subcutaneous insulin injection or infusion. The use of a second driving force is crucial to realizing the therapeutic promise of macroencapsulated islet transplantation.

This study unequivocally establishes that dependence on diffusion presents an insurmountable obstacle in the field of islet transplantation, and the introduction of an additional driving force, such as modest applied pressure, has the potential to overcome this limitation, enabling precise physiological insulin dosing. However, several substantial challenges must be addressed to translate this approach to pre-clinical studies. Notably, adapting the encapsulation device to ensure long-term viability is a critical consideration, as islet viability is a significant hurdle for clinical translation. Recent advancements, including prevascularization[41–43], the use of a collagen matrix[44,45], as well as convective flow[46–48], have improved engrafted cell viability, with islet survival demonstrated up to 80 weeks. To ensure long-term islet viability and prevent hypoxia in the days following transplantation, the implantation device used in this study must be adapted to incorporate these approaches. Importantly, the pressure-driven release approach described here is not confined to specific membranes and exhibits broad applicability, as our results have shown its efficacy to membranes with various pore sizes and porosities. While this work does not directly address the challenge of long-term engraftment viability, it can be combined with optimized islet encapsulation systems to promote long-term graft survival while enabling sub-minute insulin dosing.

METHODS

Tradeoffs between membrane area and bolus release time for diffusion-based insulin delivery

We used Fick's diffusion equation to relate the required diffusion time to release a bolus of insulin with a fixed membrane area. Consider an implant with open membrane area of A and volume of V. The time constant for this diffusion-based process is

$$\tau = \frac{Vh}{AD_S} \tag{3}$$

and the amount of insulin released in one time constant corresponds to the total amount of insulin in the implant times $1 - e^{-1}$. Suppose W_{bolus} denotes the amount of bolus insulin and W_{islet} denotes the amount of insulin secreted by an islet. We have the following relationship:

$$\frac{V}{W_{bolus}} = \frac{V_{islet}}{W_{islet}(1 - e^{-1})} \tag{4}$$

where V_{islet} is the volume occupied by an islet. Thus, we obtain the relationship between membrane area and bolus release time:

$$\tau A = \frac{W_{bolus} V_{islet}}{W_{islet}(1 - e^{-1})} \frac{h}{D_S}. \tag{5}$$

Assuming an insulin bolus of $W_{bolus} \sim 0.8 \times 10^{-6}$ g, insulin provided per islet of $W_{islet} \sim 6 \times 10^{-11}$ g, $V_{islet} \sim 4 \times 10^{-11}$ m^3, the first factor on the right side of Eq. S3 is $\sim 5 \times 10^{-7}$. We also assume a porous PET with typical thickness and porosity ($h \sim 10^{-5}$ m, 10% porosity). We use the established insulin diffusion coefficient $D_S \sim 1.5 \times 10^{-10}$ m^2/s[49]. Assuming a fixed membrane area of 1 cm^2, we can solve for the time constant:

$$\tau = \frac{W_{bolus} V_{islet}}{AW_{islet}(1 - e^{-1})} \frac{h}{D_S}. \tag{6}$$

Substituting all values gives a time constant of ~5000 seconds, ~3 hours for 90% insulin release. Similary, for a human insulin bolus of $W_{bolus} \sim 0.0325 \times 10^{-3}$ g (approximately 1 unit of insulin), insulin provided per islet of $W_{islet} \sim 6 \times 10^{-11}$ g, $V_{islet} \sim 4 \times 10^{-11}$ m^3, the first factor on the right side of Eq. S3 is ~ 0.000023. This total implant volume is in agreement with volume used for direct non-encapsulated islet transplants[50]. We assume the same membrane porosity and thickness ($h \sim 10^{-5}$ m, 10% porosity). Assuming a fixed area of 5 × 5 cm^2, and substituting all values into Eq. 6, we find a time constant of ~9,000 seconds, > 6 hours for 90% insulin release.

Derivation of multiplicative effect of applied pressure relative to diffusion for insulin transport

We start by considering the combined effect of a concentration and a pressure gradient on solute transport across a porous membrane. The combined insulin flux is dependent on flux due to solute diffusional flow, and volumetric solvent flow. This is given by

$$J_s = J_v c_s - D_s \nabla c_s. \tag{7}$$

The solute diffusional flow $-D_s \nabla c_s$ is driven by the insulin concentration gradient, D_s is the solute specific diffusion coefficient, and ∇c_s is the concentration gradient. The insulin flux, $J_v c_s$, due to solvent flow is pressure-dependent, with J_v given by

$$J_v = -L_p h \nabla p. \tag{8}$$

Here, L_p is the filtration coefficient and h is the membrane thickness. We can substitute Eq. S6 into Eq. S5 and yield

$$J_s = -L_p h \nabla p \cdot c_s - D_s \nabla c_s. \tag{9}$$

Considering a one-dimensional problem for equation Eq. 9, normalized to membrane thickness, we obtain

$$J_s = -L_p \frac{dp}{dx} c_s - \frac{D_s}{h} \frac{dc_s}{dx}. \tag{10}$$

Under steady state conditions, the fluxes due to both pressure and concentration gradients are independent of x. This gives a homogeneous second order differential equation:

$$\frac{d^2 c_s}{dx^2} - P_e \frac{dc_s}{dx} = 0 \tag{11}$$

Solving the differential equation in Eq. 11 gives

$$c_s = a e^{P_e x} + b. \tag{12}$$

Applying the boundary conditions, we can solve for a and b:

$$a = -\frac{\left(c_{s,in} - c_{s,out}\right) e^{-P_e}}{1 - e^{-P_e}} \tag{13}$$

$$b = \frac{c_{s,in} - c_{s,out} e^{-P_e}}{1 - e^{-P_e}}. \tag{14}$$

Substituting our solution for c_s to Eq. 7, with $P_e = \frac{L_p h \Delta p}{D_s}$ gives

$$J_s = J_v \frac{c_{s,in} - c_{s,out} e^{-P_e}}{1 - e^{-P_e}}. \tag{15}$$

We then take the ratio of combined pressure and diffusion transport to diffusion only transport to yield Eq. 1 in the main text.

Expressing axial Peclet number in terms of applied pressure and membrane properties

The axial Peclet number is given by

$$P_e = \frac{L_p h \Delta p}{D_s}. \tag{16}$$

We can apply the Hagen-Poiseuille Law to obtain

$$L_p = \frac{\varepsilon}{\tau} \frac{{r_p}^2}{8\eta h} \tag{17}$$

where ε is the porosity, τ is the tortuosity, and r_p is the pore radius of the membrane, h is the membrane thickness, and η is the viscosity of water. For insulin transport where membrane pore radius (r_p) is much greater than molecular radius of insulin (r_s), we can apply the Stokes-Einstein equation to obtain

$$D_s \approx \frac{\varepsilon}{\tau} \frac{k_B T}{6\pi\eta r_s} \tag{18}$$

where k_B is the Boltzmann constant and T is the absolute temperature. Plugging Eq. 17, 18 into Eq. 16, and simplifying yield Eq. 2 in the main text.

Design of the PET membrane cell culture insert

Cell culture inserts for 12-well plates were designed (FreeCAD) and 3D printed (Fictiv PLA) (Supplementary Fig. 1). Cell culture inserts included a 9-mm diameter circular opening for membrane attachment, as well as 2-mm diameter tapered circular opening for tubing. PET membranes (Sterlitech PET0413100, PET0213100, PET0813100, Falcon 353180) were attached to the cell culture insert with polyester adhesive (Hotmelt Infinity IM-Supertac-500-12). Wells in a 12-well cell culture plate were filled with 3 mL of media or water. The cell culture inserts were placed in the plate wells to wet the membranes.

Insulin transfer measurements over PET membrane, alginate-based encapsulation, and TheraCyte™ device

PET membrane cell culture inserts were placed in a 12-well cell culture plate and loaded with insulin (diluted in Milli-Q water). For diffusion measurements, samples were collected from the fluid in the cell culture plate at time points from 0 to 4 hours. For pressure-based measurements, tubing was connected to a piezoelectric pump, which was used to generate pressure difference

across a membrane. Total pump fluid for these experiments was 1 mL. Samples were also collected from the fluid in the cell culture plate at time points from 0 to 30 seconds to determine insulin recovery. Insulin content was measured by ELISA (ALPCO STELLUX 80-INSMR-CH01).

For alginate-based encapsulation, alginate was formed by curing either 0.5% or 1% sodium alginate (diluted in Milli-Q water) in calcium chloride (diluted in Milli-Q water). A metal mesh was attached to the bottom of the cell culture inserts, with polyester adhesive (Hotmelt Infinity IM- Supertac-500-12). The metal mesh was soaked in the alginate solution for 5 minutes. The coated membrane was then moved to the calcium chloride solution for 30 minutes.

TheraCyte™ devices were soaked in Milli-Q water, followed by 70% ethanol, and then followed by Milli-Q water, as per manufacturer specifications. Insulin (diluted in Milli-Q water) was then loaded into a Hamilton syringe, and injected into TheraCyte™ device, following manufacturer specifications. A 6-well cell culture plate was loaded with 3 mL of water. The loaded TheraCyte™ device was placed in the cell culture plate.

R7T1 pseudoislets culture and formation

Immortalized mouse R7T1 β-cells were cultured in DMEM high glucose containing 4 mM L-glutamine and 1 mM sodium pyruvate, with 10% FBS , 1% penicillin/streptomycin, and 1 mg/mL doxycycline (Sigma-Aldrich, St. Louis, MO, USA). R7T1 cells (passage number 10–34) were growth arrested for 5 days with doxycycline-free R7T1 medium supplemented with tetracycline free fetal bovine serum (Gibco A4736301). To form pseudoislets, growth arrested R7T1 cells were plated at 300,000 cells per well in a 12-well non-adherent plate and after 16–24 hours, pseudoislets were picked and counted for experiments.

R7T1 cells were characterized by comparing growth arrested and proliferating insulin secretion. Cells were growth arrested for 5 days by removing doxycycline from culture media. Proliferating cells were not growth arrested and were culture in media supplemented with doxycycline for the five day period. 300,000 cells per well were plated in a 12 well cell culture plate and cultured in DMEM low glucose (with or without doxycycline) for 24 hours. Media was then replaced with high glucose media and supernatant samples were collected after 30 minutes. Insulin content in supernatant was evaluated by rodent insulin ELISA (ALPCO STELLUX 80-INSMR-CH01).

***In vitro* insulin experiments with cells**

To measure insulin levels *in vitro*, R7T1 pseudoislets (~800) were loaded onto pre-wetted PET-cell culture inserts. For KCl stimulation experiments, potassium chloride was dosed inside the cell culture insert to achieve a final concentration of 40 mM. After 15 minutes, media samples were collected from inside encapsulation to measure total secreted insulin. Diffusion samples were collected from the media in the cell culture plate. For insulin release by applied pressure, a piezoelectric pump and controller were connected to the cell culture insert, and were turned on for

30 seconds, using a total volume of 1-mL, with pressure of 11 kPa. After the pump was turned off, a sample was collected from the media in the cell culture plate. The volume of media outside encapsulation was also measured. Insulin concentration was measured by ELISA (ALPCO STELLUX 80-INSMR-CH01), and total released insulin was calculated. For non-stimulated experiments, samples were collected after 8 hours of islet encapsulation, and volume was measured. For multiple time point experiments, the cell culture insert was then moved to a well with fresh DMEM, and the same protocol for insulin release was followed 2 additional times.

Human islet information and culture

Primary islets from post-mortem human donors were obtained from the Alberta Diabetes Institute (ADI) IsletCore as de-identified autopsy tissue under guidelines approved by the Stanford University Administrative Panel on Biosafety. Islet isolation was approved by the Human Research Ethics Board at the University of Alberta (Pro00013094). All donors' families gave informed consent for the use of pancreatic tissue in research. In addition, primary islets were obtained from the Integrated Islet Distribution Program (IIDP) and were used in preliminary work and supplementary viability data. Human islets were cultured overnight in islet medium before experiments. Donor information is described in Supplementary Table 1, 2.

Islet viability experiments

Human islets were encapsulated and cultured in 12-well plates for a period of 5 days. The pressure treatment group was treated with 11 kPa of applied pressure for 30 seconds every 24 hours. Encapsulated human islets in the diffusion or pressure group were collected, trypsinized, and stained with trypan blue (catalogue) to count cell death. Cell viability was measured on day 1, 3 and 5, and normalized to day 0.

Mouse islet isolation

Primary mouse islets were isolated from WT C57BL/6J mice (6–12 weeks of age) by pancreatic perifusion as previously described[51]. Briefly, mouse pancreata were perfused with Cizyme RI (VitaCyte), digested at 37°C for 13 minutes, and islets were purified in 5:6 mixture of Histopaque®-1077 and 1119. Isolated islets were collected from the interface, filtered through a 70-µm cell strainer, and cultured overnight in islet medium (5.6 mmol/L DMEM low glucose containing 4 mmol/L L-glutamine and 1 mmol/L sodium pyruvate, with 10% FBS and 1% penicillin/streptomycin) before selection for experiments.

Non-survival dosing experiments using wild type mice or mice with diabetes

For non-survival experiments, we accumulated insulin *in vitro* (~1000 ng) before islet implantation. Mouse islets, human islets, or R7T1 pseudoislets were suspended in 300-µL DMEM

in a non-adherent cell culture dish, supplemented with 1 IU/mL penicillin, 1 μg/mL streptomycin, 1 mM sodium pyruvate, 150 nM Forskolin (R7T1 pseudoislets), and 20 nM exendin-4 (mouse and human islets) for 10 hours. Conditioned media was sampled. Insulin content was measured by ELISA (ALPCO STELLUX 80-INSMR-CH01). The incubation period for the ELISA was 2 hours. The islet/pseudoislet suspension was then diluted to a concentration of 5 μg/mL. The suspension was mixed thoroughly by pipetting, and encapsulated in a 3D printed implant with PET (Sterlitech PET0413100) seal. Implants were designed (FreeCAD) and 3D printed in PLA (Fictiv). Inserts included a 9-mm diameter circular opening for membrane attachment, as well as 2-mm diameter tapered circular opening for tubing (for pressure dosed implants).

C57BL/J6 mice (10–12 weeks of age) or STZ induced diabetic C57BL/6J mice (8–10 weeks of age) were anesthetized in 2% isoflurane. Starting blood glucose was 100–180 mg/dL for WT mice, and > 400 mg/dL for diabetic mice. After anesthesia, blood glucose rose to an average of 286 mg/dL in WT mice and 553 mg/dL in diabetic mice. Protectant eye gel was applied. Animals were dosed 500 μL of 0.9% sterile saline intraperitoneally. We placed the animal on a 37˚C heat source and monitored its breathing rate throughout the procedure. We used electric clippers to remove hair on the back, from the scapulae to the hind quarters, and prepared the shaved skin by wiping with iodine, followed by isopropyl alcohol (repeating 3 times). We made a ~1.5-cm incision in the skin on the back and used a blunt probe to create space between the skin and the fascia, and then replaced the skin flap. Then, we measured blood glucose every 5 minutes using a glucometer until blood glucose was stabilized (3 consecutive readings with < 10% variation). The implant with encapsulated cells, insulin or sham control media was inserted under the skin and tubing was routed to exit the incision caudally. After replacing the skin flap, we closed the incision with surgical staples (Fine Science Tools 12022-09). Insulin dosing was performed immediately after implantation. For pressure-treated cases (and sham control), the tubing was connected to a piezoelectric pump, to generate a pressure difference across the PET membrane of 11 kPa for 30 seconds. No pumping was performed for the diffusion cases. At 0, 15, 30, and 60 minutes, blood glucose was measured using a glucometer and blood samples were collected from the tail vein. Plasma was separated from red blood cells by centrifuging at 10000 RPM. Breath rate was measured at each time point and was > 30 per minute for all mice.

After 60–90 minutes, the implant was recovered from the animal. A sample of conditioned media was collected, to be used to measure remaining insulin content. Islets were removed from conditioned media by centrifuging at 2000 rpm for 2 minutes and collecting supernatant. Plasma insulin content, as well as remaining insulin in encapsulated conditioned media were measured by ELISA (ALPCO STELLUX 80-INSMR-CH01). If animals did not survive, the data was not included in presented results.

STZ diabetes induction and monitoring

Eight-week-old male C57BL/6J mice were fasted for 4–6 hours. Immediately prior to injection, streptozotocin was suspended in 100-mM sterile sodium citrate buffer (pH 4.5). Mice were injected

intraperitoneally with 175 mg/kg streptozotcin[52,53] for non-survival experiments, or 150 mg/kg for survival experiments. For three days following injection, drinking water was supplemented with 10% sucrose to prevent hypoglycemia. Once animals reached hyperglycemia (a non-fasting blood glucose > 350mg/dL for several measurements), they were used for insulin dosing experiments. All mice were used for experiments within 1 week of streptozotocin injection. When blood glucose reached > 450 mg/dL, mice were dosed 0.05–0.1 unit of insulin subcutaneously daily. The last insulin dose was given no sooner than 14 hours before an experiment (survival or non-survival).

Survival dosing experiments

For survival experiments, *in vitro* culture was used to rest islets after isolation, before transplantation. Freshly isolated mouse islets were cultured in 1000-µL DMEM in a non-adherent cell culture dish, supplemented with 1 IU/mL penicillin, 1 µg/mL streptomycin, and 1 mM sodium pyruvate for ~10 hours. ~400 islets were then manually picked and moved to fresh DMEM supplemented with 1 IU/mL penicillin, 1 µg/mL streptomycin, 1 mM sodium pyruvate, and 20 nM exendin-4. The suspension was mixed thoroughly by pipetting and encapsulated in a 3D printed implant as previously described.

STZ induced Diabetic C57BL/6J mice (8–10 weeks of age) were anesthetized in 2% isoflurane. The implantation procedures are identical to those described in non-survival dosing experiments. After implantation, the animal was placed in a recovery cage on a 37˚C heat source and provided with food and water. Blood glucose was measured using a glucometer once per hour for 6 hours. After 6 hours, the first insulin dose was delivered. Animals were anesthetized briefly (~30 seconds). For pressure-driven-dosing animals, and sham controls, the tubing was connected to a piezoelectric pump, which was used to generate a pressure difference across the PET membrane of 11 kPa for 30 seconds. At 0, 15, 30, and 60 minutes, blood glucose was measured using a glucometer. Blood glucose was then monitored once every hour for 6 hours. A second dose was performed, as described above, and blood glucose was measured at 0, 15, 30 and 60 minutes. Blood glucose was then monitored every hour for 6 hours. Animals were provided food and water throughout the full experiment. Once the final blood glucose measurement was taken, the animals were anesthetized with isoflurane and euthanized through cervical dislocation.

In the basal dosing experiments, we began by bringing the blood glucose levels to the euglycemic range by injecting a single subcutaneous dose of 0.05 units of Humalog. Subsequently, we administered 2.5 seconds of dosing every 30 minutes. Throughout the experiment, the animals were freely moving, and no anesthesia was required after the initial surgery. Once the final blood glucose measurement was taken, the animals were anesthetized with isoflurane and euthanized through cervical dislocation.

Design of piezoelectric pump controller and wearable wireless micropump

Pizeoelectric micropumps (Servoflo mp6-liq/ mp6-hyb) were used for all pressure-driven experiments. A pump driver and controller were designed. An electroluminescent lamp circuit (Microchip HV861) was used as a complimentary dual output piezoelectric driver. Pump rate was calibrated by characterizing the frequency, duty cycle and flow rate relationship.

For the wearable wireless micropump, a wireless module (Fanstel BC832) was used to control the piezoelectric driver. Duty cycle was used to adjust the pump rate, and pump time was set by user from a smartphone user interface. A single lithium ion (CR1616) battery was used for power. Silicone tubing (McMaster 2124T2) was connected to the pump, and a reservoir was fabricated out of polyolefin (Pointool PO-01450) and connected to the tubing. Pump fluid consisted of either saline or cell culture media. We optimized the power consumption and the weight of the whole system to allow wild type and STZ induced diabetic mice to comfortably carry the full system. The miniaturized system was then packaged in a wearable pouch fabricated out of cotton (Fig. 5E).

Pump pressure was characterized by using a differential pressure sensor (NXP MPX2102DP), with full scale pressure of 100 kPa. Pump outlet was connected to pressure sensor inlet using silicone tubing (McMaster 2124T3). The pump was turned on and the output voltage was measured. Pressure was then calculated based off sensor specifications and measured output voltage. For system pressure measurements, an encapsulation implant was 3D printed (Fictiv PLA) with two openings for silicone tubing. A porous PET membrane was sealed to the open side of the encapsulation implant. One tube was connected to the pump outlet and one tube was connected to the pressure sensor inlet. The pump was turned on, and pressure was measured as described above.

Statistical analysis

All statistical tests were performed using GraphPad Prism software (GraphPad Software Inc.). Statistical significance was assessed using either Student's t-test or one-way ANOVA. P-values indicating the significance levels between conditions are reported as $*P < 0.05$, $**P < 0.01$, $***P < 0.001$, and $****P < 0.0001$. Data is represented as mean +/- standard error. The experimental results were independently validated for each dataset presented in this study.

References

1. Perkins, B. A., Sherr, J. L. & Mathieu, C. Type 1 diabetes glycemic management: Insulin therapy, glucose monitoring, and automation. *Science* **373**, 522–527 (2021).
2. Addala, A. *et al.* A Decade of Disparities in Diabetes Technology Use and HbA1c in Pediatric Type 1 Diabetes: A Transatlantic Comparison. *Diabetes Care* **44**, 133–140 (2021).
3. Lal, R. A., Ekhlaspour, L., Hood, K. & Buckingham, B. Realizing a Closed-Loop (Artificial Pancreas) System for the Treatment of Type 1 Diabetes. *Endocr Rev* **40**, 1521–1546 (2019).
4. Ryan, E. A. *et al.* Clinical outcomes and insulin secretion after islet transplantation with the Edmonton protocol. *Diabetes* **50**, 710–719 (2001).
5. Shapiro, A. M. J. *et al.* International trial of the Edmonton protocol for islet transplantation. *N Engl J Med* **355**, 1318–1330 (2006).
6. Ryan, E. A. *et al.* Five-year follow-up after clinical islet transplantation. *Diabetes* **54**, 2060–2069 (2005).
7. Markmann, J. F. *et al.* 259-OR: Stem Cell–Derived, Fully Differentiated Islet Cells for Type 1 Diabetes. *Diabetes* **71**, 259-OR (2022).
8. Reichman, T. W. *et al.* 836-P: Glucose-Dependent Insulin Production and Insulin-Independence in Type 1 Diabetes from Stem Cell–Derived, Fully Differentiated Islet Cells—Updated Data from the VX-880 Clinical Trial. *Diabetes* **72**, 836-P (2023).
9. Ashimova, A., Yegorov, S., Negmetzhanov, B. & Hortelano, G. Cell Encapsulation Within Alginate Microcapsules: Immunological Challenges and Outlook. *Front Bioeng Biotechnol* **7**, 380 (2019).
10. Kobayashi, T. *et al.* Indefinite islet protection from autoimmune destruction in nonobese diabetic mice by agarose microencapsulation without immunosuppression1. *Transplantation* **75**, 619–625 (2003).
11. Veiseh, O. *et al.* Size- and shape-dependent foreign body immune response to materials implanted in rodents and non-human primates. *Nat Mater* **14**, 643–651 (2015).
12. Ramzy, A. *et al.* Implanted pluripotent stem-cell-derived pancreatic endoderm cells secrete glucose-responsive C-peptide in patients with type 1 diabetes. *Cell Stem Cell* **28**, 2047-2061.e5 (2021).
13. Shapiro, A. M. J. *et al.* Insulin expression and C-peptide in type 1 diabetes subjects implanted with stem cell-derived pancreatic endoderm cells in an encapsulation device. *Cell Rep Med* **2**, 100466 (2021).

14. Pepper, A. R. *et al.* Diabetes Is Reversed in a Murine Model by Marginal Mass Syngeneic Islet Transplantation Using a Subcutaneous Cell Pouch Device. *Transplantation* **99**, 2294–2300 (2015).
15. Bachul, P. J. *et al.* 306-OR: Modified Approach for Improved Islet Allotransplantation into Prevascularized Sernova Cell Pouch Device: Preliminary Results of the Phase I/II Clinical Trial at University of Chicago. *Diabetes* **71**, 306-OR (2022).
16. Kumagai-Braesch, M. *et al.* The TheraCyte™ device protects against islet allograft rejection in immunized hosts. *Cell Transplant* **22**, 1137–1146 (2013).
17. Boettler, T. *et al.* Pancreatic Tissue Transplanted in TheraCyte Encapsulation Devices Is Protected and Prevents Hyperglycemia in a Mouse Model of Immune-Mediated Diabetes. *Cell Transplant* **25**, 609–614 (2016).
18. Sweet, I. R. *et al.* Treatment of diabetic rats with encapsulated islets. *J Cell Mol Med* **12**, 2644–2650 (2008).
19. Bruin, J. E. *et al.* Maturation and function of human embryonic stem cell-derived pancreatic progenitors in macroencapsulation devices following transplant into mice. *Diabetologia* **56**, 1987–1998 (2013).
20. Ludwig, B. *et al.* Transplantation of human islets without immunosuppression. *Proc Natl Acad Sci U S A* **110**, 19054–19058 (2013).
21. Ludwig, B. *et al.* A novel device for islet transplantation providing immune protection and oxygen supply. *Horm Metab Res* **42**, 918–922 (2010).
22. Carlsson, P.-O. *et al.* Transplantation of macroencapsulated human islets within the bioartificial pancreas βAir to patients with type 1 diabetes mellitus. *Am J Transplant* **18**, 1735–1744 (2018).
23. An, D. *et al.* Designing a retrievable and scalable cell encapsulation device for potential treatment of type 1 diabetes. *Proc Natl Acad Sci U S A* **115**, E263–E272 (2018).
24. Wang, X. *et al.* A nanofibrous encapsulation device for safe delivery of insulin-producing cells to treat type 1 diabetes. *Sci Transl Med* **13**, eabb4601 (2021).
25. Hwa, A. J. & Weir, G. C. Transplantation of Macroencapsulated Insulin-Producing Cells. *Curr Diab Rep* **18**, 50 (2018).
26. Korsgren, O. Islet Encapsulation: Physiological Possibilities and Limitations. *Diabetes* **66**, 1748–1754 (2017).
27. Omer, A. *et al.* Exercise Induces Hypoglycemia in Rats With Islet Transplantation. *Diabetes* **53**, 360–365 (2004).

28. Krawczyk, K. *et al.* Electrogenetic cellular insulin release for real-time glycemic control in type 1 diabetic mice. *Science* **368**, 993–1001 (2020).

29. Ader, M., Pacini, G., Yang, Y. J. & Bergman, R. N. Importance of Glucose Per Se to Intravenous Glucose Tolerance. *Diabetes* **34**, 1092–103 (1985).

30. Ader, M., Ni, T. C. & Bergman, R. N. Glucose effectiveness assessed under dynamic and steady state conditions. Comparability of uptake versus production components. *J. Clin. Invest.* **99**, 1187–1199 (1997).

31. Korsgren, E. & Korsgren, O. Glucose Effectiveness: The Mouse Trap in the Development of Novel ß-Cell Replacement Therapies. *Transplantation* **100**, 111–115 (2016).

32. Bruce, C. R. *et al.* Translating glucose tolerance data from mice to humans: Insights from stable isotope labelled glucose tolerance tests. *Mol Metab* **53**, 101281 (2021).

33. Trivedi, N., Steil, G. M., Colton, C. K., Bonner-Weir, S. & Weir, G. C. Improved vascularization of planar membrane diffusion devices following continuous infusion of vascular endothelial growth factor. *Cell Transplant* **9**, 115–124 (2000).

34. Ahrén, B. & Pacini, G. Glucose effectiveness: Lessons from studies on insulin-independent glucose clearance in mice. *J of Diabetes Invest* **12**, 675–685 (2021).

35. Barkai, U. *et al.* Enhanced oxygen supply improves islet viability in a new bioartificial pancreas. *Cell Transplant* **22**, 1463–1476 (2013).

36. Piezoelectric Micro Pumps - Takasago Fluidic Systems. https://www.takasago-fluidics.com/pages/piezoelectric-micro-pumps.

37. Piezoelectric Pump. https://www.dolomite-microfluidics.com/product/piezoelectric-pump/.

38. mp6 Micropump - Pressure Sensors - Mass Flow Sensors - Humidity Sensors - Micropumps. https://www.servoflo.com/micropumps/mp6/mp6-micropump.

39. Nalbach, L. *et al.* Improvement of islet transplantation by the fusion of islet cells with functional blood vessels. *EMBO Mol Med* **13**, e12616 (2021).

40. Mathieu, C., Gillard, P. & Benhalima, K. Insulin analogues in type 1 diabetes mellitus: getting better all the time. *Nat Rev Endocrinol* **13**, 385–399 (2017).

41. Mridha, A. R. *et al.* Prevascularized Retrievable Hybrid Implant to Enhance Function of Subcutaneous Encapsulated Islets. *Tissue Eng Part A* **28**, 212–224 (2022).

42. Skrzypek, K. *et al.* An important step towards a prevascularized islet macroencapsulation device—effect of micropatterned membranes on development of endothelial cell network. *J Mater Sci: Mater Med* **29**, 91 (2018).

43. Pepper, A. R. *et al.* A prevascularized subcutaneous device-less site for islet and cellular transplantation. *Nat Biotechnol* **33**, 518–523 (2015).

44. Harrington, S., Williams, J., Rawal, S., Ramachandran, K. & Stehno-Bittel, L. Hyaluronic Acid/Collagen Hydrogel as an Alternative to Alginate for Long-Term Immunoprotected Islet Transplantation <sup/>. *Tissue Engineering Part A* **23**, 1088–1099 (2017).

45. Riopel, M. & Wang, R. Collagen matrix support of pancreatic islet survival and function. *Front Biosci (Landmark Ed)* **19**, 77–90 (2014).

46. Song, S. *et al.* Silicon nanopore membrane (SNM) for islet encapsulation and immunoisolation under convective transport. *Sci Rep* **6**, 23679 (2016).

47. Song, S. *et al.* An intravascular bioartificial pancreas device (iBAP) with silicon nanopore membranes (SNM) for islet encapsulation under convective mass transport. *Lab Chip* **17**, 1778–1792 (2017).

48. Yang, K. *et al.* A therapeutic convection–enhanced macroencapsulation device for enhancing β cell viability and insulin secretion. *Proc Natl Acad Sci USA* **118**, e2101258118 (2021).

49. Shorten, P. R., McMahon, C. D. & Soboleva, T. K. Insulin Transport within Skeletal Muscle Transverse Tubule Networks. *Biophysical Journal* **93**, 3001–3007 (2007).

50. Rickels, M. R. & Robertson, R. P. Pancreatic Islet Transplantation in Humans: Recent Progress and Future Directions. *Endocrine Reviews* **40**, 631–668 (2019).

51. Lee, S. *et al.* β-Cell Succinate Dehydrogenase Deficiency Triggers Metabolic Dysfunction and Insulinopenic Diabetes. *Diabetes* **71**, 1439–1453 (2022).

52. Deeds, M. C. *et al.* Single dose streptozotocin-induced diabetes: considerations for study design in islet transplantation models. *Lab Anim* **45**, 131–140 (2011).

53. Furman, B. L. Streptozotocin-Induced Diabetic Models in Mice and Rats. *Curr Protoc Pharmacol* **70**, 5.47.1-5.47.20 (2015).

Acknowledgments

We are thankful to the Alberta Diabetes Institute IsletCore at the University of Alberta in Edmonton with the assistance of the Human Organ Procurement and Exchange (HOPE) program, Trillium Gift of Life Network (TGLN), and other Canadian organ procurement organizations for their support in providing human islets.

Funding

Stanford Bio-X Interdisciplinary Initiatives Seed Grants Program (IIP) (R10-56) (ASYP, JPA)
IIDP NIH Grant # 2UC4DK098085 (JPA, ASYP)
Stanford SystemX (ASYP)
NIH R01DK101530 (JPA)
NIH R01DK119955 (JPA)
Stanford Graduate Fellowship and Stanford Bio-X Bowes Fellowship (EAT)
Pilot and Feasibility grant from the Stanford Diabetes Research Center, NIH P30DK116074 (SL)
NIH T32 DK007217 (RL, SL)

Author contributions

EAT performed the experiments, interpreted the data, conceptualized the study, designed the experiments, and wrote the manuscript. RAL conceptualized the study, interpreted the data, and edited the manuscript. HX performed the experiments, designed the experiments, and edited the manuscript. SL performed the experiments and edited the manuscript. HM designed the experiments, interpreted the data, and edited the manuscript. JPA conceptualized the study, designed the experiments, interpreted the data, and wrote the manuscript. ASYP conceptualized the study, designed the experiments, interpreted the data, and wrote the manuscript.

Competing Interests

Authors declare that they have no competing interests.

Data and materials availability

All data are available in the main text or the supplementary materials.

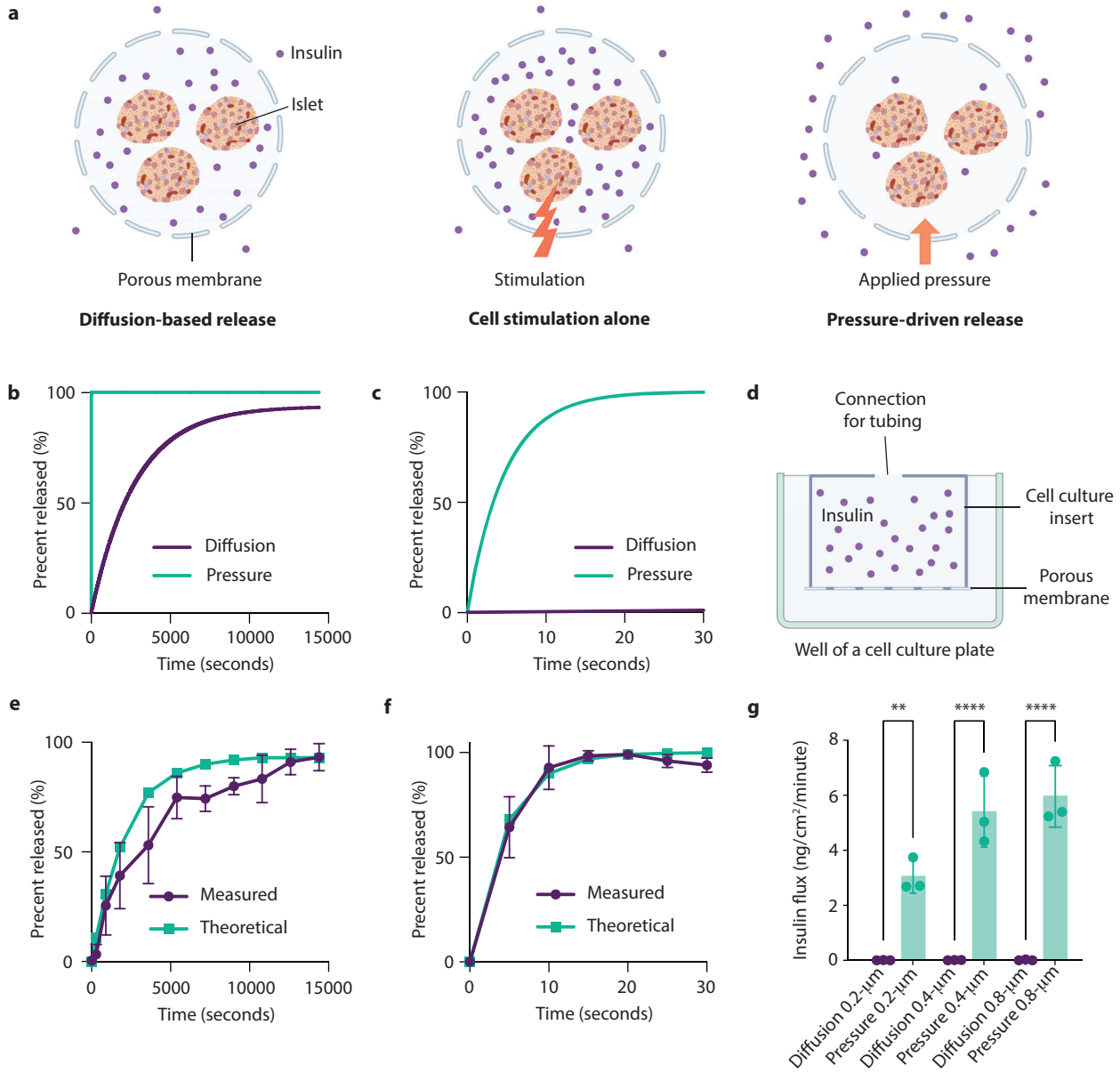

Fig. 1. Importance of a second driving force—small pressure gradient—for sub-minute insulin transport across a porous membrane. a, Illustrations of insulin movement from within the macroencapsulated islet environment through a porous membrane based on diffusion alone, diffusion plus stimulated insulin release, and an applied pressure. **b**, Theoretical calculations of the percentage of insulin transported across the membrane from diffusion alone and a small (11 kPa) pressure gradient. **c**, Zoom in of (**b**) over the first 30 seconds. **d**, Experimental set-up for measuring insulin levels within and outside the porous membrane-contained space. **e**, **f**, Empirical measurements of insulin transport for diffusion alone (**e**) and pressure-driven (**f**) as compared with theoretical calculations for a 0.4-mm pore size membrane. **g**, Empirical measurement of insulin flux for pore sizes of 0.2 mm (9.4% porosity), 0.4 mm (12.6% porosity), and 0.8 mm (15.1% porosity). $^{**}P < 0.01$, $^{****}P < 0.0001$.

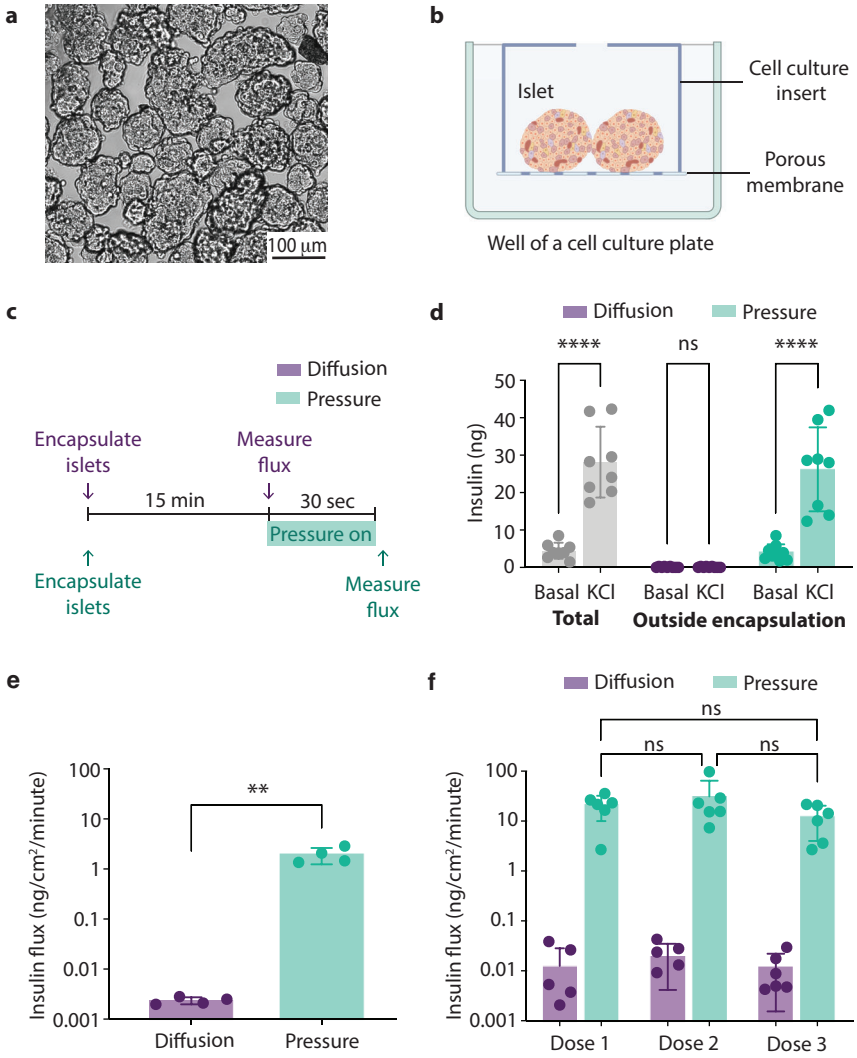

Fig. 2. *In vitro* validation of pressure-driven dosing across a porous membrane supporting repeated insulin boluses. a, Brightfield image of R7T1 pseudoislets. **b**, Experimental set-up for measuring insulin levels released from encapsulated R7T1 pseudoislets within and outside the porous membrane-contained space. **c**, Experimental procedure for KCl stimulated and basal insulin secretion from encapsulated R7T1 pseudoislets with (green) and without (purple) an applied pressure. **d**, Measurements of total insulin released (both inside and outside of encapsulation), and insulin transported to the outside of encapsulation by diffusion and applied pressure for KCl stimulated and basal R7T1 pseudoislets. **e**, Comparison of insulin flux by diffusion and pressure driven delivery for basal R7T1 pseudoislets over 8 hours. **f**, Insulin flux comparison from three sequential *in vitro* bolus generations at 8-hour intervals. $^{**}P < 0.01$, $^{****}P < 0.0001$.

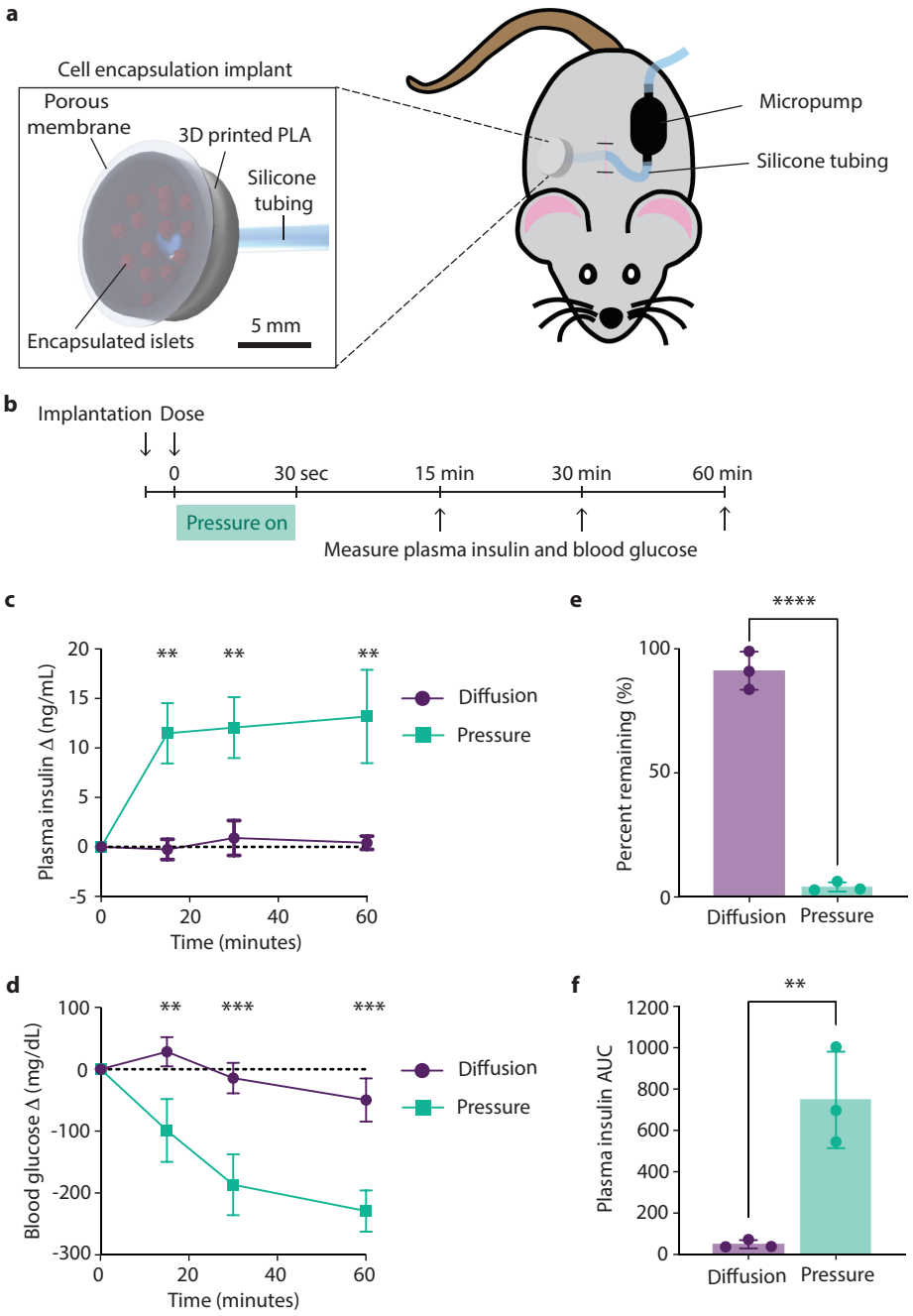

Fig. 3. Pressure-driven dosing from macroencapsulated islets supporting physiologic insulin dosing in WT mice. a, Anesthetized mouse with cell encapsulation implant and micropump connected *via* silicone tubing. PLA, polylactic acid. **b**, Experimental timeline: insulin was dosed almost immediately after implantation and a ~11-kPa pressure was applied for 30 seconds for pressured-treated mice. Blood glucose was measured and blood samples were collected at 0, 15, 30, and 60 minutes after initial insulin dosing. **c**, Blood insulin increase in mice treated with either diffusion or applied pressure, n = 3/group. **d**, Blood glucose drop in mice treated with either diffusion or applied pressure, n = 3/group. **e**, Percentage of dosed insulin

remaining in implant after 90 minutes, $n = 3$/group. **f**, Blood insulin AUC in mice treated with either pressure or diffusion, $n = 3$/group. $^{**}P < 0.01$, $^{***}P < 0.001$, $^{****}P < 0.0001$.

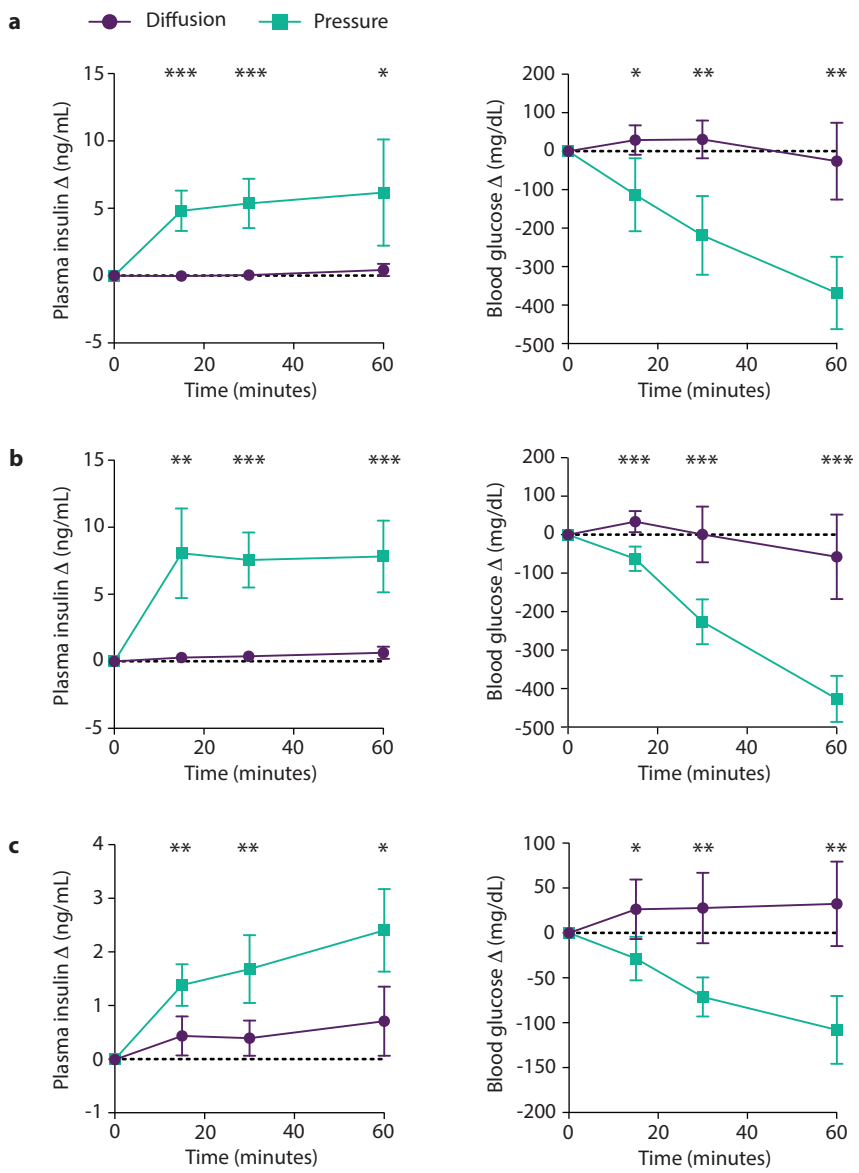

Fig. 4. Restoring euglycemia in diabetic mice through pressure-driven insulin dosing. a to **c**, Plasma insulin and blood glucose changes in mice dosed with diffusion (purple) or pressure-driven (green) insulin release from encapsulated (**a**) mouse islets, (**b**) human islets, and (**c**) R7T1 pseudoislets. $n = 5$/group. *$P < 0.05$, **$P < 0.01$, ***$P < 0.001$.

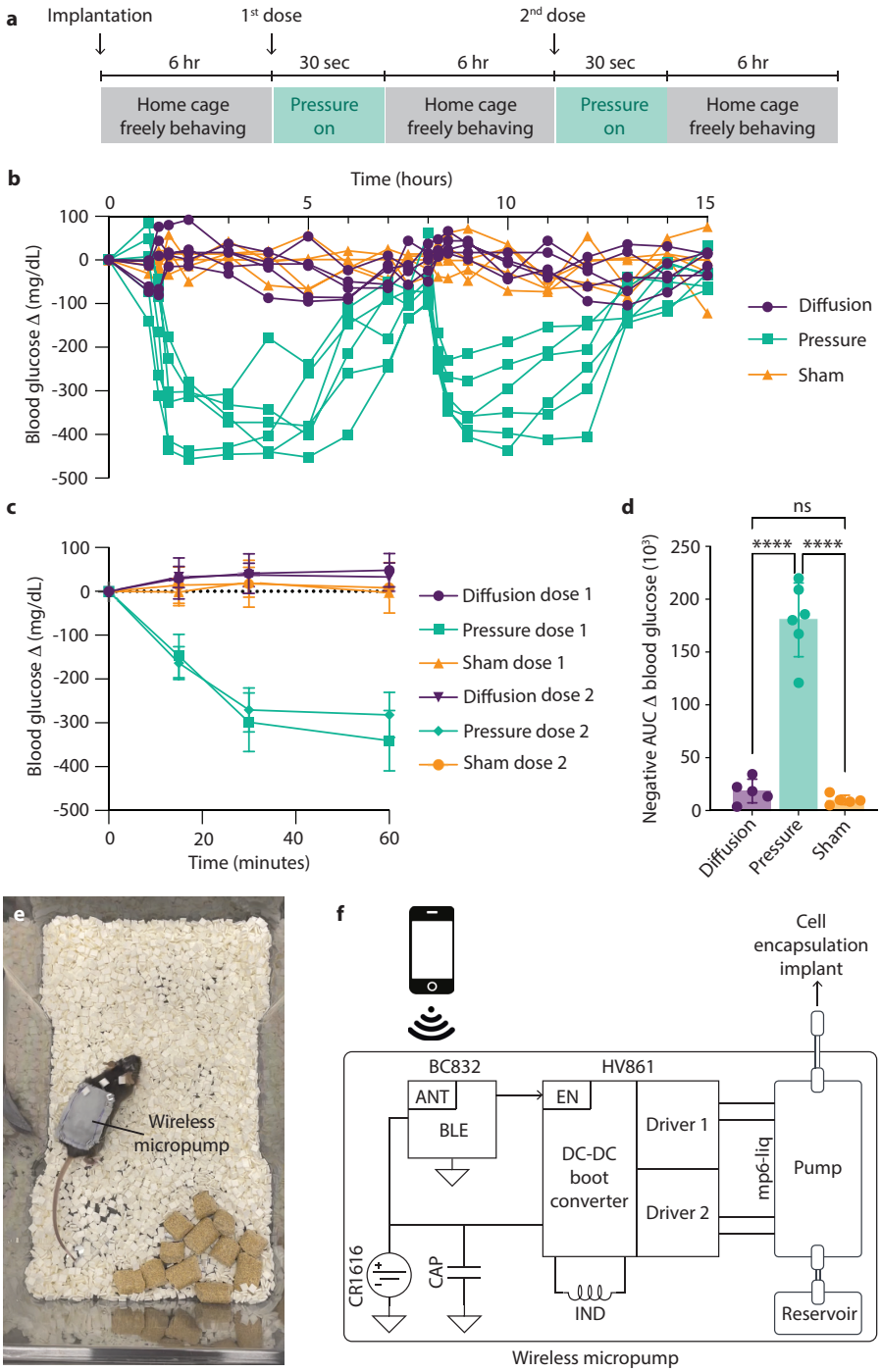
a
Implantation
1st dose
2nd dose
6 hr
30 sec
6 hr
30 sec
6 hr
Home cage freely behaving
Pressure on
Home cage freely behaving
Pressure on
Home cage freely behaving
b
Time (hours)
Blood glucose Δ (mg/dL)
Diffusion
Pressure
Sham
c
Blood glucose Δ (mg/dL)
Time (minutes)
Diffusion dose 1
Pressure dose 1
Sham dose 1
Diffusion dose 2
Pressure dose 2
Sham dose 2
d
ns
****
****
Negative AUC Δ blood glucose (10³)
Diffusion
Pressure
Sham
e
Wireless micropump
f
Cell encapsulation implant
BC832
HV861
ANT
BLE
EN
DC-DC boot converter
Driver 1
Driver 2
mp6-liq
Pump
CR1616
CAP
IND
Reservoir
Wireless micropump
G
Implantation
Injection
6 hr
6 hr
Home cage freely behaving
Pressure on 2.5 s every 30 min
H
Time (hours)
Blood glucose Δ (mg/dL)
Pressure
Sham

Fig. 5. Comparing glycemic control in diabetic mice with repeated pressure-driven insulin boluses or basal insulin delivery. **a**, Experimental procedure for insulin boluses experiments. **b**, Blood glucose changes in animals treated with either diffusion, applied pressure, or sham transplanted controls. Diffusion and sham, $n = 5$/condition; Pressure, $n = 6$. **c**, Blood glucose deltas in 60 minutes following delivery of the first and second doses. Diffusion and sham, $n = 5$/condition; Pressure, $n = 6$. **d**, Blood glucose delta AUC in animals treated by diffusion, applied pressure, and sham transplanted controls. Diffusion and sham, $n = 5$/condition; Pressure, $n = 6$. **e**, Photograph of the wireless micropump system on a mouse. **f**, Architecture of the wireless micropump system. The system includes a high-voltage dual driver (part no. HV861), a Bluetooth transceiver module with an integrated antenna (ANT), a piezoelectric micropump (part no. mp6-liq), and a coin battery (CR1616). **g**, Timeline for basal dosing experiments. **h**, Basal blood glucose changes in animals treated with Humalog injection or Humalog injection combined with pressure-based dosing. Pressure, $n = 4$; Sham $n = 5$. ****$P < 0.0001$.